



Isospin-breaking corrections to superallowed Fermi β decay in isospin- and angular-momentum-projected nuclear density functional theory

W. Satuła,^{1,*} J. Dobaczewski,^{1,2} W. Nazarewicz,^{1,3,4} and T. R. Werner¹

¹*Institute of Theoretical Physics, Faculty of Physics, University of Warsaw, ul. Hoża 69, PL-00-681 Warsaw, Poland*

²*Department of Physics, P.O. Box 35 (YFL), University of Jyväskylä, FI-40014 Jyväskylä, Finland*

³*Department of Physics and Astronomy, University of Tennessee, Knoxville, Tennessee 37996, USA*

⁴*Physics Division, Oak Ridge National Laboratory, P.O. Box 2008, Oak Ridge, Tennessee 37831, USA*

(Received 4 October 2012; published 26 November 2012)

Background: Superallowed β -decay rates provide stringent constraints on physics beyond the standard model of particle physics. To extract crucial information about the electroweak force, small isospin-breaking corrections to the Fermi matrix element of superallowed transitions must be applied.

Purpose: We perform systematic calculations of isospin-breaking corrections to superallowed β decays and estimate theoretical uncertainties related to the basis truncation, to time-odd polarization effects related to the intrinsic symmetry of the underlying Slater determinants, and to the functional parametrization.

Methods: We use the self-consistent isospin- and angular-momentum-projected nuclear density functional theory employing two density functionals derived from the density-independent Skyrme interaction. Pairing correlations are ignored. Our framework can simultaneously describe various effects that impact matrix elements of the Fermi decay: symmetry breaking, configuration mixing, and long-range Coulomb polarization.

Results: Isospin-breaking corrections to the $I = 0^+$, $T = 1 \rightarrow I = 0^+$, $T = 1$ pure Fermi transitions are computed for nuclei from $A = 10$ to $A = 98$ and, for the first time, to the Fermi branch of the $I, T = 1/2 \rightarrow I, T = 1/2$ transitions in mirror nuclei from $A = 11$ to $A = 49$. We carefully analyze various model assumptions impacting theoretical uncertainties of our calculations and provide theoretical error bars on our predictions.

Conclusions: The overall agreement with empirical isospin-breaking corrections is very satisfactory. Using computed isospin-breaking corrections we show that the unitarity of the CKM matrix is satisfied with a precision of better than 0.1%.

DOI: [10.1103/PhysRevC.86.054316](https://doi.org/10.1103/PhysRevC.86.054316)

PACS number(s): 21.10.Hw, 21.60.Jz, 21.30.Fe, 23.40.Hc

I. INTRODUCTION

By studying isotopes with an enhanced sensitivity to fundamental symmetries, nuclear physicists can test various aspects of the standard model in ways that are complementary to other sciences. For example, a possible explanation for the observed asymmetry between matter and antimatter in the universe could be studied by searching for a permanent electric dipole moment larger than standard model predictions in heavy radioactive nuclei that have permanent octupole shapes. Likewise, the superallowed β decays of a handful of rare isotopes with similar numbers of protons and neutrons, in which both the parent and the daughter nuclear states have zero angular momentum and positive parity, are a unique laboratory to study the strength of the weak force.

What makes these pure vector-current-mediated (Fermi) decays so useful for testing the standard model is the hypothesis of the conserved vector current (CVC), that is, independence of the vector current on the nuclear medium. The consequence of the CVC hypothesis is that the product of the statistical rate function f and partial half-life t for the superallowed $I = 0^+$, $T = 1 \rightarrow I = 0^+$, $T = 1$ Fermi β decay should be nucleus independent and

equal to

$$ft = \frac{K}{G_V^2 |M_F^{(\pm)}|^2} = \text{const}, \quad (1)$$

where $K/(\hbar c)^6 = 2\pi^3 \hbar \ln 2 / (m_e c^2)^5 = 8120.2787(11) \times 10^{-10} \text{ GeV}^{-4} \text{ s}$ is a universal constant; G_V stands for the vector coupling constant for semileptonic weak interactions, and $M_F^{(\pm)}$ is the nuclear matrix element of the isospin rising or lowering operator \hat{T}_{\pm} .

Relation (1) does not hold exactly and must be slightly amended by introducing a set of radiative corrections to the ft values and a correction to the nuclear matrix element owing to isospin symmetry breaking:

$$|M_F^{(\pm)}|^2 = 2(1 - \delta_C) \quad (2)$$

(see Refs. [1–4], and references cited therein). Because these corrections are small, of the order of a percent, they can be approximately factorized and arranged in the following way:

$$\mathcal{F}t \equiv ft(1 + \delta'_R)(1 + \delta_{NS} - \delta_C) = \frac{K}{2G_V^2(1 + \Delta_R^V)}, \quad (3)$$

with the left-hand side being nucleus independent. In Eq. (3), $\Delta_R^V = 2.361(38)\%$ stands for the nucleus-independent part of the radiative correction [5], δ'_R is a transition-dependent (Z -dependent) but nuclear-structure-independent part of the radiative correction [2,5], and δ_{NS} denotes the nuclear-structure-dependent part of the radiative correction [2,6].

* wojciech.satula@fuw.edu.pl

In spite of theoretical uncertainties in the evaluation of radiative and isospin-symmetry-breaking corrections, the superallowed β decay is the most precise source of experimental information for determining the vector coupling constant G_V and provides us with a stringent test of the CVC hypothesis. In turn, it is also the most precise source of the matrix element $V_{ud} = G_V/G_\mu$ of the Cabibbo-Kobayashi-Maskawa (CKM) three-generation quark mixing matrix [2,7–9]. This is so because the leptonic coupling constant, $G_\mu/(\hbar c)^3 = 1.16637(1) \times 10^{-5} \text{ GeV}^{-2}$, is well known from the muon decay [9].

The advantage of the superallowed β -decay strategy results from the fact that, within the CVC hypothesis, V_{ud} can be extracted by averaging over several transitions in different nuclei. For precise tests of the standard model, only these transitions that have ft values known with a relative precision better than a fraction of a percent are acceptable. Currently, 13 “canonical” transitions spreading over a wide range of nuclei, from $A = 10$ to $A = 74$, meet this criterion (have ft values measured with an accuracy of order 0.3% or better) and are used to evaluate the values of G_V and V_{ud} [2].

In this work we concentrate on the isospin-breaking (ISB) corrections δ_C that were already computed by various authors using a diverse set of nuclear models [2,10–17]. The standard in this field has been set by Towner and Hardy (HT) [2], who used the nuclear shell model to account for the configuration mixing effect and the mean-field (MF) approach to account for a radial mismatch of proton and neutron single-particle (s.p.) wave functions caused by Coulomb polarization. In this study, which constitutes an extension of our earlier work [15], we use the isospin- and angular-momentum-projected density functional theory (DFT). This method can account, in a rigorous quantum-mechanical way, for spontaneous symmetry-breaking (SSB) effects, configuration mixing, and long-range Coulomb polarization effects.

Our paper is organized as follows. The model is described in Sec. II. The results of calculations for ISB corrections to the superallowed $0^+ \rightarrow 0^+$ Fermi transitions are summarized in Sec. III. ISB corrections to the Fermi matrix elements in mirror-symmetric $T = 1/2$ nuclei are discussed in Sec. IV. Section V studies a particular case of the Fermi decay of ^{32}Cl . Finally, a summary and perspectives are given in Sec. VI.

II. THE MODEL

The success of the self-consistent DFT approach to mesoscopic systems [18], in general, and to atomic nuclei [19–21], in particular, has its roots in the SSB mechanism that incorporates essential short-range (pairing) and long-range (spatial) correlations within a single deformed Slater determinant. The deformed states provide a basis for the symmetry-projected DFT approaches, which aim at including beyond-MF correlations through the restoration of broken symmetries by means of projection techniques [22].

A. Isospin- and angular-momentum-projected DFT approach

The building block of the isospin- and angular-momentum-projected DFT approach employed in this study is the self-

consistent deformed MF state $|\varphi\rangle$, which violates both the rotational and the isospin symmetries. While the rotational invariance is of a fundamental nature and is broken spontaneously, the isospin symmetry is violated both spontaneously and explicitly by the Coulomb interaction between protons. The strategy is to restore the rotational invariance, remove the spurious isospin mixing caused by the isospin SSB effect, and retain only the physical isospin mixing owing to the electrostatic interaction [23,24]. This is achieved by a re-diagonalization of the entire Hamiltonian, consisting of the isospin-invariant kinetic energy and Skyrme force and the isospin-non-invariant Coulomb force, in a basis that conserves both angular momentum and isospin.

To this end, we first find the self-consistent MF state $|\varphi\rangle$ and then build a normalized angular-momentum- and isospin-conserving basis $|\varphi; IMK; TT_z\rangle$ by using the projection method,

$$|\varphi; IMK; TT_z\rangle = \frac{1}{\sqrt{N_{\varphi;IMK;TT_z}}} \hat{P}_{T_z, T_z}^T \hat{P}_{M, K}^I |\varphi\rangle, \quad (4)$$

where \hat{P}_{T_z, T_z}^T and $\hat{P}_{M, K}^I$ stand for the standard isospin and angular-momentum projection operators,

$$\hat{P}_{T_z, T_z}^T = \frac{2T+1}{2} \int_0^\pi dT_z (\beta_T) \hat{R}(\beta_T) \sin \beta_T d\beta_T, \quad (5)$$

$$\hat{P}_{M, K}^I = \frac{2I+1}{8\pi^2} \int D_{MK}^I(\Omega) \hat{R}(\Omega) d\Omega, \quad (6)$$

where $\hat{R}(\beta_T) = e^{-i\beta_T \hat{T}_y}$ is the rotation operator about the y axis in the isospace, $d_{T_z, T_z}^T(\beta_T)$ is the Wigner function, and $T_z = (N - Z)/2$ is the third component of the total isospin T . As usual, $\hat{R}(\Omega) = e^{-i\gamma \hat{J}_z} e^{-i\beta \hat{J}_y} e^{-i\alpha \hat{J}_z}$ is the three-dimensional rotation operator in space, $\Omega = (\alpha, \beta, \gamma)$ are the Euler angles, $D_{MK}^I(\Omega)$ is the Wigner function, and M and K denote the angular-momentum components along the laboratory and intrinsic z axis, respectively [22,25]. Note that unpaired MF states $|\varphi\rangle$ conserve the third isospin component T_z ; hence, the one-dimensional isospin projection suffices.

The set of states (4) is, in general, overcomplete because the K quantum number is not conserved. This difficulty is overcome by selecting first the subset of linearly independent states known as the *collective space* [22], which is spanned, for each I and T , by the so-called *natural states* $|\varphi; IM; TT_z\rangle^{(i)}$ [26,27]. The entire Hamiltonian—including the ISB terms—is re-diagonalized in the collective space, and the resulting eigenfunctions are

$$|n; \varphi; IM; T_z\rangle = \sum_{i, T \geq |T_z|} a_{iIT}^{(n; \varphi)} |\varphi; IM; TT_z\rangle^{(i)}, \quad (7)$$

where the index n labels the eigenstates in ascending order according to their energies. The amplitudes $a_{iIT}^{(n; \varphi)}$ define the degree of isospin mixing through the so-called isospin-mixing coefficients (or isospin impurities), determined for a given n th eigenstate as

$$\alpha_C^n = 1 - \sum_i |a_{iIT}^{(n; \varphi)}|^2, \quad (8)$$

where the sum of norms corresponds to the isospin T dominating in the wave function $|n; \varphi; IM; T_z\rangle$.

One of the advantages of the projected DFT compared to shell-model-based approaches [2,28] is that it allows for a rigorous quantum-mechanical evaluation of the Fermi matrix element using the bare isospin operators,

$$\hat{T}_{\pm} = \frac{1}{2} \sum_{k=1}^A (\hat{t}_x^{(k)} \pm i \hat{t}_y^{(k)}) \equiv \mp \frac{1}{2} \hat{T}_{1\pm 1}, \quad (9)$$

where $\hat{T}_{1\pm 1}$ denotes the rank 1 covariant one-body spherical-tensor operators in the isospace (see discussion in Ref. [29]). Indeed, noting that each m th eigenstate, (7), can be uniquely decomposed in terms of the original basis states, (4),

$$|m; \varphi; IM; T_z\rangle = \sum_{K,T} f_{KT}^{(\varphi; m, I)} \hat{P}_{T_z, T_z}^T \hat{P}_{M, K}^I |\varphi\rangle, \quad (10)$$

with microscopically determined mixing coefficients $f_{KT}^{(\varphi; m, I)}$, the expression for the Fermi matrix element between the parent state $|m; \varphi; IM; T_z\rangle$ and the daughter state $|n; \psi; IM; T_z \pm 1\rangle$ can be written as

$$\begin{aligned} & \langle m; \varphi; IM; T_z | \hat{T}_{\mp} | n; \psi; IM; T_z \pm 1 \rangle \\ &= \pm \frac{1}{2} \sum_{TT'} \sum_{KK'} f_{KT}^{(\varphi; m, I)*} f_{K'T'}^{(\psi; n, I)} \\ & \quad \times \langle \varphi | \hat{P}_{T_z, T_z}^T \hat{T}_{1\mp 1} \hat{P}_{T_z \pm 1, T_z \pm 1}^{T'} \hat{P}_{K, K'}^I | \psi \rangle \\ &= \pm \frac{2I+1}{16\pi^2} \sum_{TT'} \sum_{KK'} f_{KT}^{(\varphi; m, I)*} f_{K'T'}^{(\psi; n, I)} \int d\Omega D_{KK'}^{I*}(\Omega) \\ & \quad \times \langle \varphi | \hat{P}_{T_z, T_z}^T \hat{T}_{1\mp 1} \hat{P}_{T_z \pm 1, T_z \pm 1}^{T'} | \tilde{\psi} \rangle, \end{aligned} \quad (11)$$

where the tilde indicates the Slater determinant rotated in space: $|\tilde{\psi}\rangle = |\psi(\Omega)\rangle = \hat{R}(\Omega)|\psi\rangle$. The matrix element appearing on the right-hand side of Eq. (11) can be expressed through the transition densities, which are basic building blocks of the multireference DFT [24,30–32]. Indeed, with the aid of the identity

$$\hat{P}_{K, M}^T \hat{T}_{\lambda, \mu} \hat{P}_{M', K'}^{T'} = C_{T'M' \lambda \mu}^{TM} \sum_{\nu=-\lambda}^{\lambda} C_{T'K-\nu \lambda \nu}^{TK} \hat{T}_{\lambda \nu} \hat{P}_{K-\nu, K'}^{T'}, \quad (12)$$

which results from the general transformation rule for spherical tensors under rotations or isorotations,

$$\hat{R}(\Omega) \hat{T}_{\lambda \mu} \hat{R}(\Omega)^\dagger = \sum_{\mu'} D_{\mu' \mu}^\lambda(\Omega) \hat{T}_{\lambda \mu'}, \quad (13)$$

the matrix element entering Eq. (11) can be expressed as

$$\begin{aligned} & \langle \varphi | \hat{P}_{T_z, T_z}^T \hat{T}_{1\mp 1} \hat{P}_{T_z \pm 1, T_z \pm 1}^{T'} | \tilde{\psi} \rangle \\ &= C_{T'T_z \pm 1 1 \mp 1}^{TT_z} \sum_{\nu} C_{T'T_z - \nu 1 \nu}^{TT_z} \langle \varphi | \hat{T}_{1 \nu} \hat{P}_{T_z - \nu, T_z \pm 1}^{T'} | \tilde{\psi} \rangle. \end{aligned} \quad (14)$$

For unpaired Slater determinants considered here, the double integral over the isospace Euler angles in Eq. (11) can be further reduced to a one-dimensional integral over the angle β_T using the identity

$$\hat{T}_{\lambda \mu} e^{i\alpha \hat{T}_z} = e^{-i\alpha \mu} e^{i\alpha \hat{T}_z} \hat{T}_{\lambda \mu}, \quad (15)$$

which is the one-dimensional version of the transformation rule, (13), valid for rotations around the Oz axis in the isospace.

The final expression for the matrix element in Eq. (14) reads

$$\begin{aligned} & \langle \varphi | \hat{T}_{1 \nu} \hat{P}_{T_z - \nu, T_z \pm 1}^{T'} | \tilde{\psi} \rangle \\ &= \frac{2T'+1}{2} \int_0^\pi d\beta_T \sin \beta_T d_{T_z - 1, T_z \pm 1}^{T'} \langle \varphi | \hat{T}_{1 \nu} e^{-i\beta_T \hat{T}_y} | \tilde{\psi} \rangle \\ &= (-1)^\nu \frac{2T'+1}{2} \int_0^\pi d\beta_T \sin \beta_T d_{T_z - 1, T_z \pm 1}^{T'} \mathcal{N}(\Omega, \beta_T) \\ & \quad \times \int d^3 \mathbf{r} \tilde{\rho}_{1-\nu}(\Omega, \beta_T, \mathbf{r}), \end{aligned} \quad (16)$$

where $\tilde{\rho}_{1\nu}(\Omega, \beta_T, \mathbf{r})$ is the isovector transition density, and the double-tilde sign indicates that the right Slater determinant used to calculate this density is rotated both in space and in isospace: $|\tilde{\psi}\rangle = \hat{R}(\beta_T) \hat{R}(\Omega) |\psi\rangle$. The symbol $\mathcal{N}(\Omega, \beta_T) = \langle \varphi | \hat{R}(\beta_T) \hat{R}(\Omega) | \psi \rangle$ denotes the overlap kernel.

Because natural states have good isospin, the states (7) are free from spurious isospin mixing. Moreover, because the isospin projection is applied to self-consistent MF solutions, our model accounts for a subtle balance between long-range Coulomb polarization, which tends to make proton and neutron wave functions different, and short-range nuclear attraction, which acts in the opposite way. Long-range polarization affects globally all s.p. wave functions. Direct inclusion of this effect in open-shell heavy nuclei is possible essentially only within the DFT, which is the only *no-core* microscopic framework that can be used there.

Recent experimental data on the isospin impurity deduced in ^{80}Zr from giant dipole resonance γ -decay studies [33] agree well with the impurities calculated using isospin-projected DFT based on modern Skyrme-force parametrizations [16,23]. This further demonstrates that the isospin-projected DFT is capable of capturing the essential piece of physics associated with isospin mixing.

B. The choice of Skyrme interaction

As discussed in Ref. [24], the isospin projection technique outlined above does not yield singularities in energy kernels; hence, it can be safely executed with all commonly used energy density functionals (EDFs). However, as demonstrated in Ref. [14], the isospin projection alone leads to unphysically large isospin mixing in odd-odd $N = Z$ nuclei. It has thus been concluded that—in order to obtain reasonable results— isospin projection must be augmented by angular-momentum projection. This not only increases the numerical effort, but also brings back the singularities in the energy kernels [14] and thus prevents one from using the modern parametrizations of the Skyrme EDFs, which all contain density-dependent terms [34]. Therefore, the only option [14] is to use the Hamiltonian-driven EDFs. For Skyrme-type functionals, this leaves us with one choice: the SV parametrization [35]. In order to better control the time-odd fields, the standard SV parametrization must be augmented by the tensor terms, which were neglected in the original work [35].

This density-independent parametrization of the Skyrme functional has an isoscalar effective mass as low as $\frac{m^*}{m} \approx 0.38$, which is required to reproduce the actual nuclear saturation properties. The unusual saturation mechanism of SV has a

TABLE I. Skyrme parameters t_i , x_i ($i = 0, 1, 2, 3$), and W of SV [35] and SHZ2. The last column shows relative changes in parameters. Both parametrizations use the nucleon-mass parameter of $\hbar^2/2m = 20.73$ MeV fm². Parameters not listed are equal to 0.

| Parameter | SV | SHZ2 | Change (%) |
|-----------|-----------|-------------|------------|
| t_0 | -1248.290 | -1244.98830 | -0.26 |
| t_1 | 970.560 | 970.01156 | -0.06 |
| t_2 | 107.220 | 99.50197 | -7.20 |
| x_0 | -0.170 | 0.01906 | -111.21 |
| W | 150 | 150 | 0 |

dramatic impact on the overall spectroscopic quality of this force, impairing such key properties as the symmetry energy [14], level density, and level ordering. These deficiencies also affect the calculated isospin mixing, which is a prerequisite for realistic estimates of δ_C . In particular, in the case of ⁸⁰Zr discussed above, SV yields $\alpha_C \approx 2.8\%$, which is considerably smaller than the mean value of $\bar{\alpha}_C \approx 4.4\% \pm 0.3\%$ obtained by averaging over nine popular Skyrme EDFs, the MSk1, SkO', SkP, SLy4, SLy5, SLy7, SkM*, SkXc, and SIII functionals (see Ref. [16] for further details). Even though the ISB corrections δ_C are primarily sensitive to *differences* between isospin mixing in isobaric analog states, the lack of a reasonable Hamiltonian-based Skyrme EDF is probably the most critical deficiency of the current formalism.

The aim of this study is (i) to provide the most reliable set of ISB corrections that can be obtained within the current angular-momentum and isospin-projected single-reference DFT and (ii) to explore the sensitivity of results to EDF parameters, choice of particle-hole configurations, and structure of time-odd fields, which correlate valence neutron-proton pairs in odd-odd $N = Z$ nuclei. In particular, to quantify uncertainties related to the Skyrme coupling constants, we have developed a new density-independent variant of the Skyrme force, hereafter dubbed SHZ2 (see Table I).

The force was optimized purposefully to properties of light magic nuclei below ¹⁰⁰Sn. The coupling constants t_0 , t_1 , t_2 , and x_0 of SHZ2 were found by means of a χ^2 minimization to experimental [36] binding energies of five doubly magic nuclei: ¹⁶O, ⁴⁰Ca, ⁴⁸Ca, ⁵⁶Ni, and ¹⁰⁰Sn. The procedure reduced the χ^2 from ~ 6.0 for the SV set to ~ 3.6 for SHZ2. Most of the nuclear matter characteristics calculated for both sets are similar. It appears, however, that the fit to light nuclei only weakly constrains the symmetry energy. The bulk symmetry energy of SHZ2 is $a_{\text{sym}} \approx 42.2$ MeV, i.e., it overestimates the accepted value $a_{\text{sym}} \approx 32 \pm 2$ MeV by almost 30%. While this property essentially precludes using SHZ2 in detailed nuclear structure studies, it also creates an interesting opportunity for investigating the quenching of ISB effects owing to the large isospin-symmetry-restoring components of the force.

C. Numerical details

All calculations presented below were done using the code HFODD [26,37], version (2.48q) or higher, which includes both angular-momentum and isospin projections. In order

to obtain converged results for isospin mixing with respect to basis truncation, in our SV calculations we used $N = 10$ harmonic oscillator (HO) shells for $A < 40$ nuclei, 12 shells for $40 \leq A < 62$ nuclei, and 14 shells for $A \geq 62$ nuclei. In SHZ2 test calculations, we took $N = 10$ shells for $A < 40$ and $N = 12$ shells for $A > 40$ nuclei.

For numerical integration over the Euler angles in space and isospace ($\alpha, \beta, \gamma; \beta_T$), we used the Gauss-Chebyshev (over α and γ) and Gauss-Legendre (over β and β_T) quadratures. We took $n_\alpha = n_\beta = n_\gamma = 20$ and $n_{\beta_T} = 8$ (or 10) integration points. This choice guarantees that the calculated values of δ_C are not affected by the numerical integration error.

III. ISB CORRECTIONS TO SUPERALLOWED $0^+ \rightarrow 0^+$ FERMION TRANSITIONS

The $0^+ \rightarrow 0^+$ Fermi β decay proceeds between the ground state (g.s.) of the even-even nucleus $|I = 0, T \approx 1, T_z = \pm 1\rangle$ and its isospin-analog partner in the $N = Z$ odd-odd nucleus, $|I = 0, T \approx 1, T_z = 0\rangle$. The corresponding transition matrix element is

$$M_F^{(\pm)} = \langle I = 0, T \approx 1, T_z = \pm 1 | \hat{T}_\pm | I = 0, T \approx 1, T_z = 0 \rangle. \quad (17)$$

The g.s. $|I = 0, T \approx 1, T_z = \pm 1\rangle$ in Eq. (17) is approximated by a projected state,

$$|I = 0, T \approx 1, T_z = \pm 1\rangle = \sum_{T \geq 1} c_T^{(\psi)} \hat{P}_{\pm 1, \pm 1}^T \hat{P}_{0,0}^{I=0} |\psi\rangle, \quad (18)$$

where $|\psi\rangle$ is the g.s. of the even-even nucleus obtained in self-consistent MF calculations. The state $|\psi\rangle$ is unambiguously defined by filling in the pairwise doubly degenerate levels of protons and neutrons up to the Fermi level. The daughter state $|I = 0, T \approx 1, T_z = 0\rangle$ is approximated by

$$|I = 0, T \approx 1, T_z = 0\rangle = \sum_{T \geq 0} c_T^{(\varphi)} \hat{P}_{0,0}^T \hat{P}_{0,0}^{I=0} |\varphi\rangle, \quad (19)$$

where the self-consistent Slater determinant $|\varphi\rangle \equiv |\bar{\nu} \otimes \pi\rangle$ (or $|\nu \otimes \bar{\pi}\rangle$) represents the so-called antialigned configuration, selected by placing the odd neutron and the odd proton in the lowest available time-reversed (or signature-reversed) s.p. orbits. The s.p. configuration $|\bar{\nu} \otimes \pi\rangle$ manifestly breaks the isospin symmetry as schematically depicted in Fig. 1. The isospin projection from $|\varphi\rangle$ as expressed by Eq. (19) is essentially the only way to reach the $|T \approx 1, I = 0\rangle$ states in odd-odd $N = Z$ nuclei.

A. Shape-current orientation

At variance with the even-even parent nuclei, the antialigned configurations in odd-odd daughter nuclei are not uniquely defined. One of the reasons, which was not fully appreciated in our previous work [15], is related to the relative orientation of the nuclear shapes and currents associated with the valence neutron-proton pairs. In all signature-symmetry-restricted calculations for triaxial nuclei, such as ours, there

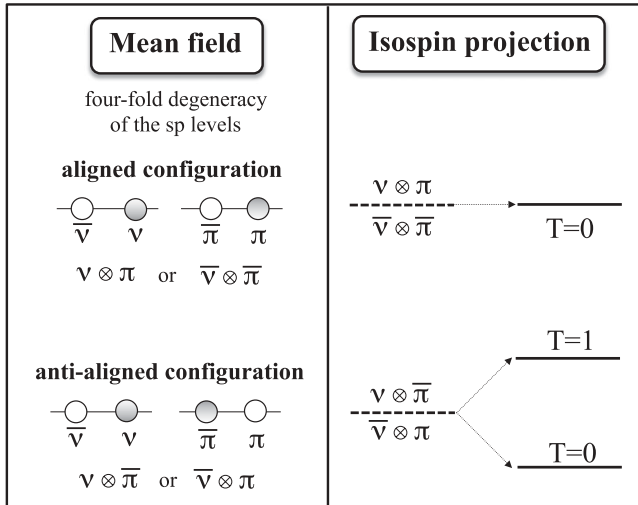


FIG. 1. Left: Two possible g.s. configurations of an odd-odd $N = Z$ nucleus, as described by the conventional deformed MF theory. These degenerate configurations are called aligned (upper) and anti-aligned (lower), depending on what levels are occupied by the valence particles. Right: What happens when the isospin symmetry is restored. The aligned configuration is isoscalar; hence, it is insensitive to the isospin projection. The anti-aligned configuration represents a mixture of $T = 0$ and $T = 1$ states. The isospin projection removes the degeneracy by lowering the $T = 0$ level.

are three anti-aligned Slater determinants, with the s.p. angular momenta (alignments) of the valence protons and neutrons pointing, respectively, along the Ox , Oy , or Oz axis of the intrinsic shape defined by means of the long (Oz), intermediate (Ox), and short (Oy) principal axes of the nuclear mass distribution. These solutions, hereafter referred to as $|\varphi_X\rangle$, $|\varphi_Y\rangle$, and $|\varphi_Z\rangle$, are schematically illustrated in Fig. 2. Their properties can be summarized as follows.

- (1) The three solutions are not linearly independent. Their Hartree-Fock (HF) binding energies may typically differ by a few hundred kilo-electron volts. The differences come almost entirely from the isovector correlations in the time-odd channel, as shown in the lower panel in Fig. 3 for the representative example of ^{34}Cl . Let us stress that

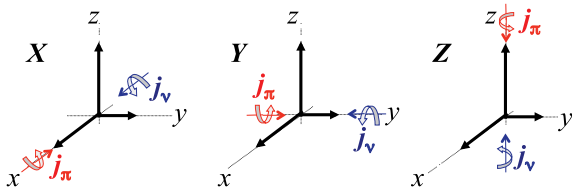


FIG. 2. (Color online) Schematic illustration of relative orientations of shapes and currents in the three anti-aligned states, $|\varphi_X\rangle$ (X), $|\varphi_Y\rangle$ (Y), and $|\varphi_Z\rangle$ (Z), discussed in the text. The long (Oz), intermediate (Ox), and short (Oy) principal axes of the nuclear mass distribution are indicated by thick arrows. The odd-neutron (j_v) and odd-proton (j_π) angular momentum oriented along the Ox , Oy , or Oz axis is shown by thin arrows. Note that in each case the total angular-momentum alignment, $j_v + j_\pi$, is 0.

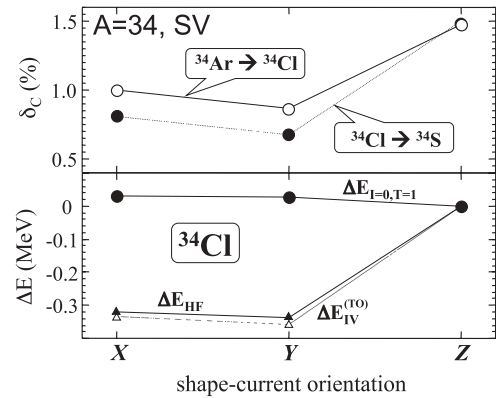


FIG. 3. Top: ISB corrections δ_C for $0^+ \rightarrow 0^+$ superallowed β decays $^{34}\text{Ar} \rightarrow ^{34}\text{Cl}$ (open circles) and $^{34}\text{Cl} \rightarrow ^{34}\text{S}$ (filled circles) determined for the shape-current orientations X , Y , and Z depicted schematically in Fig. 2. Bottom: Differences between the energies of the X and Y configurations and that of the Z configuration in ^{34}Cl . Filled triangles correspond to the total HF energies and open triangles correspond to contributions from the time-odd isovector channel. Filled circles show the total energy differences obtained for the angular-momentum and isospin-projected states.

- these poorly known correlations may significantly impact the ISB corrections, as shown in the upper panel in Fig. 3.
- (2) The type of isovector time-odd correlations captured by the HF solutions depends on the relative orientation of the nucleonic currents with respect to the nuclear shapes. Solutions oriented perpendicular to the long axis, $|\varphi_X\rangle$ and $|\varphi_Y\rangle$, are usually similar to one another (they yield identical correlations for axial systems) and differ from $|\varphi_Z\rangle$, oriented parallel to the long axis, which captures more correlations owing to the current-current time-odd interactions.
- (3) The three $|T = 1, I = 0^+\rangle$ states projected from the $|\varphi_X\rangle$, $|\varphi_Y\rangle$, and $|\varphi_Z\rangle$ Slater determinants differ in energy by only a few tens of kilo-electron volts (see the lower panel in Fig. 3). Hence, energywise, they represent the same physical solution, differing only slightly owing to polarization effects originating from different components of the time-odd isovector fields. However, because these correlations are completely absent in the even-even parent nuclei, they strongly impact the calculated δ_C . The largest differences in δ_C have been obtained for $A = 34$ and $A = 74$ systems (see Fig. 3 and Tables II and III).
- (4) Symmetry-unrestricted calculations always converge to the signature-symmetry-conserving solution $|\varphi_Z\rangle$, which, rather surprisingly, appears to be energetically unfavored (except for ^{18}F). In spite of our persistent efforts, no self-consistent tilted-axis solutions have been found.

B. Nearly degenerate K orbitals

Owing to an increased density of s.p. Nilsson levels in the vicinity of the Fermi surface for nearly spherical nuclei, another type of ambiguity appears in choosing the Slater determinants representing anti-aligned configurations. Within the set of nuclei studied in this work, this ambiguity

TABLE II. Results of calculations for superallowed transitions measured experimentally. Listed are empirical ft values [4]; SV values of δ_C calculated by projecting from the $|\varphi_X\rangle$, $|\varphi_Y\rangle$, and $|\varphi_Z\rangle$ Slater determinants (see Sec. III A); recommended mean $\delta_C^{(SV)}$ corrections (see Sec. III C) and corresponding $\mathcal{F}t$ values; empirical $\delta_C^{(exp)}$ corrections calculated using Eq. (23); contributions coming from individual transitions to the χ^2 budget in the confidence-level test; and mean $\delta_C^{(SHZ2)}$ corrections and corresponding $\mathcal{F}t$ values.

| Parent nucleus | ft (s) | $\delta_C^{(X)}$ (%) | $\delta_C^{(Y)}$ (%) | $\delta_C^{(Z)}$ (%) | $\delta_C^{(SV)}$ (%) | $\mathcal{F}t$ (s) | $\delta_C^{(exp)}$ (%) | χ_i^2 | $\delta_C^{(SHZ2)}$ (%) | $\mathcal{F}t$ (s) |
|--|-------------|-------------------------|-------------------------|-------------------------|--------------------------|-----------------------|---------------------------|--|----------------------------|-----------------------|
| $T_z = -1$ | | | | | | | | | | |
| ^{10}C | 3041.7(43) | 0.559 | 0.559 | 0.823 | 0.65(14) | 3062.1(62) | 0.37(15) | 3.7 | 0.462(65) | 3067.8(49) |
| ^{14}O | 3042.3(11) | 0.303 | 0.303 | 0.303 | 0.303(30) | 3072.3(21) | 0.36(06) | 0.8 | 0.480(48) | 3066.9(24) |
| ^{22}Mg | 3052.0(70) | 0.243 | 0.243 | 0.417 | 0.301(87) | 3080.5(75) | 0.62(23) | 1.9 | 0.342(49) | 3079.2(72) |
| ^{34}Ar | 3052.7(82) | 0.865 | 0.997 | 1.475 | 1.11(29) | 3056(12) | 0.63(27) | 3.1 | 1.08(42) | 3057(15) |
| $T_z = 0$ | | | | | | | | | | |
| ^{26}Al | 3036.9(09) | 0.308 | 0.308 | 0.494 | 0.370(95) | 3070.5(31) | 0.37(04) | 0.0 | 0.307(62) | 3072.5(23) |
| ^{34}Cl | 3049.4(11) | 0.809 | 0.679 | 1.504 | 1.00(38) | 3060(12) | 0.65(05) | 48.4 | 0.83(50) | 3065(15) |
| ^{42}Sc | 3047.6(12) | — | — | — | 0.77(27) | 3069.2(85) | 0.72(06) | 0.5 | 0.70(32) | 3071(10) |
| ^{46}V | 3049.5(08) | 0.486 | 0.486 | 0.759 | 0.58(14) | 3074.6(47) | 0.71(06) | 4.5 | 0.375(96) | 3080.9(35) |
| ^{50}Mn | 3048.4(07) | 0.460 | 0.460 | 0.740 | 0.55(14) | 3074.1(47) | 0.67(07) | 3.1 | 0.39(13) | 3079.2(45) |
| ^{54}Co | 3050.8(10) | 0.622 | 0.622 | 0.671 | 0.638(68) | 3074.0(32) | 0.75(08) | 2.0 | 0.51(20) | 3078.0(66) |
| ^{62}Ga | 3074.1(11) | 0.925 | 0.840 | 0.881 | 0.882(95) | 3090.0(42) | 1.51(09) | 44.0 | 0.49(11) | 3102.3(45) |
| ^{74}Rb | 3084.9(77) | 2.054 | 1.995 | 1.273 | 1.77(40) | 3073(15) | 1.86(27) | 0.1 | 0.90(22) | 3101(11) |
| $\overline{\mathcal{F}t} = 3073.6(12)$ | | | | | | $\chi^2 = 112.2$ | | $\overline{\mathcal{F}t} = 3075.0(12)$ | | |
| $ V_{ud} = 0.97397(27)$ | | | | | | $\chi_d^2 = 10.2$ | | $ V_{ud} = 0.97374(27)$ | | |
| 0.99935(67) | | | | | | 0.99890(67) | | | | |

manifests itself particularly strongly in ^{42}Sc , where we deal with four possible antialigned MF configurations built on the Nilsson orbits originating from the spherical $\nu f_{7/2}$ and $\pi f_{7/2}$ subshells. These configurations can be labeled in terms of the quantum number K as $|\nu \bar{K} \otimes \pi K\rangle$, with $K = 1/2, 3/2, 5/2$, and $7/2$.

In the extreme shell-model picture, each of these states contains all the $T = 1$ and $I = 0, 2, 4$, and 6 components. Within the projected DFT picture, owing to configuration-dependent polarizations in time-odd and time-even channels, the situation is more complicated because the Slater determinants $|\nu \bar{K} \otimes \pi K\rangle$ corresponding to different K values are no longer degenerate. Consequently, for each angular momentum I , one obtains four different linearly dependent solutions. Calculations show that in all $I = 0$ and $T \approx 1$ states of

interest, the isospin mixing α_C is essentially independent of the choice of the initial Slater determinant. In contrast, the calculated ISB corrections δ_C and energies depend on K (see Fig. 4).

TABLE III. Similar to Table II, except for the unmeasured transitions.

| Parent nucleus | $\delta_C^{(X)}$ (%) | $\delta_C^{(Y)}$ (%) | $\delta_C^{(Z)}$ (%) | $\delta_C^{(SV)}$ (%) | $\delta_C^{(SHZ2)}$ (%) |
|------------------|-------------------------|-------------------------|-------------------------|--------------------------|----------------------------|
| $T_z = -1$ | | | | | |
| ^{18}Ne | 2.031 | 1.064 | 1.142 | 1.41(46) | 0.72(30) |
| ^{26}Si | 0.399 | 0.399 | 0.597 | 0.47(10) | 0.529(77) |
| ^{30}S | 1.731 | 1.260 | 1.272 | 1.42(26) | 0.98(21) |
| $T_z = 0$ | | | | | |
| ^{18}F | 1.819 | 0.956 | 0.987 | 1.25(42) | 0.42(24) |
| ^{22}Na | 0.255 | 0.255 | 0.535 | 0.35(14) | 0.216(86) |
| ^{30}P | 1.506 | 0.974 | 1.009 | 1.16(27) | 0.60(20) |
| ^{66}As | 0.956 | 0.925 | 1.694 | 1.19(38) | 0.64(12) |
| ^{70}Br | 1.654 | 1.479 | 1.429 | 1.52(18) | 1.10(52) |

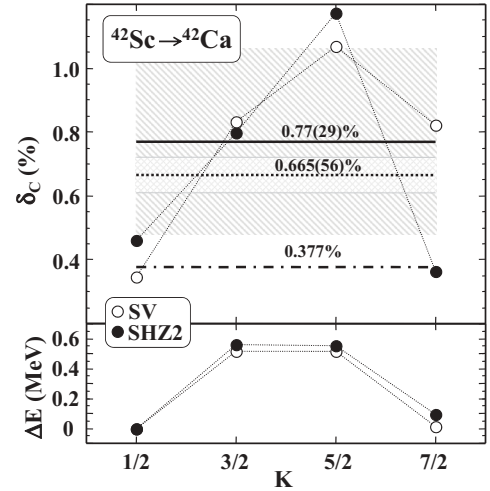


FIG. 4. Top: ISB corrections to the $^{42}\text{Sc} \rightarrow ^{42}\text{Ca}$ superallowed β transition, calculated using SV (open circles) and SHZ2 (filled circles) forces by projecting the $|\nu \bar{K} \otimes \pi K\rangle$ configurations in ^{42}Sc for $K = 1/2, 3/2, 5/2$, and $7/2$. From top to bottom, horizontal lines show (i) the average ISB correction using SV (thick solid line); (ii) the value from Ref. [2] (dotted line); and (iii) the δ_C from Ref. [12]. Shaded regions mark related uncertainties. Bottom: Projected energies of states $|K; I = 0^+, T \approx 1\rangle$ in ^{42}Sc obtained from the configurations $|\nu \bar{K} \otimes \pi K\rangle$, relative to the projected energy of the $K = 1/2$ state.

C. Theoretical uncertainties and error analysis

Based on the discussion presented in Secs. III A and III B, the recommended calculated values of δ_C for the superallowed $0^+ \rightarrow 0^+$ β decay are determined by averaging over three relative orientations of shapes and currents. Only in the case of $A = 42$ do we adopt for δ_C an arithmetic mean over the four configurations associated with different K orbitals.

To minimize uncertainties in α_C and δ_C associated with truncation of the HO basis in HFODD, we used different HO spaces in different mass regions (cf. Sec. II C). With this choice, the resulting systematic errors owing to the basis cutoff should not exceed $\sim 10\%$. To illustrate the dependence of δ_C on the number of HO shells, Fig. 5 shows the case of the superallowed $^{46}\text{V} \rightarrow ^{46}\text{Ti}$ transition obtained by projecting from the $|\varphi_Z\rangle$ solution in ^{46}V . In this case, the parent and daughter nuclei are axial, which allows us to reduce the angular-momentum projection to one dimension and extend the basis size up to $N = 20$ HO shells.

With increasing N , δ_C increases, and asymptotically it reaches the value of $0.8096(12)\%$. This limiting value is about 6.7% larger than the value of 0.7587% obtained for $N = 12$ shells, that is, for a basis used to compute the $42 \leq A \leq 54$ cases. For $62 \leq A \leq 74$ nuclei, which were all found to be triaxial, we have used $N = 14$ shells. A further increase in basis size is practically impossible. Nonetheless, as shown in Fig. 5, the rate of increase in δ_C slows down exponentially with N , which supports our 10% error estimate owing to the basis truncation.

The total error of the calculated value of δ_C includes the standard deviation from the averaging, σ_n , and the assumed 10% uncertainty owing to the basis size: $\Delta(\delta_C) = \sqrt{\sigma_n^2 + (0.1\delta_C)^2}$. The same prescription for $\Delta(\delta_C)$ was also used in the test calculations with SHZ2, even though a slightly smaller HO basis was employed in that case.

For $A = 38$ nuclei, our model predicts the unusually large correction $\delta_C \approx 10\%$. The origin of the very different isospin mixing obtained for odd-odd and even-even members of this isobaric triplet is not fully understood. Most likely, it is a consequence of the poor spectroscopic properties of SV. Indeed, as a result of the incorrect balance between the spin-orbit and the tensor terms in SV, the $2s_{1/2}$ subshell is shifted up in energy close to the Fermi surface. This state is

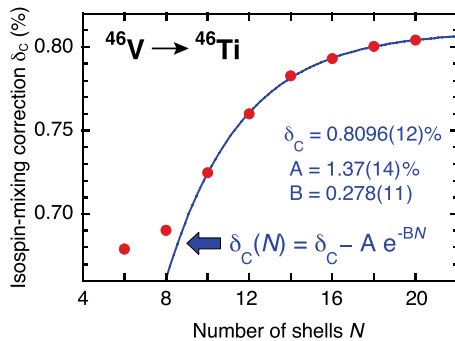


FIG. 5. (Color online) Convergence of the ISB correction δ_C to the $^{46}\text{V} \rightarrow ^{46}\text{Ti}$ superallowed β decay versus the number of oscillator shells considered.

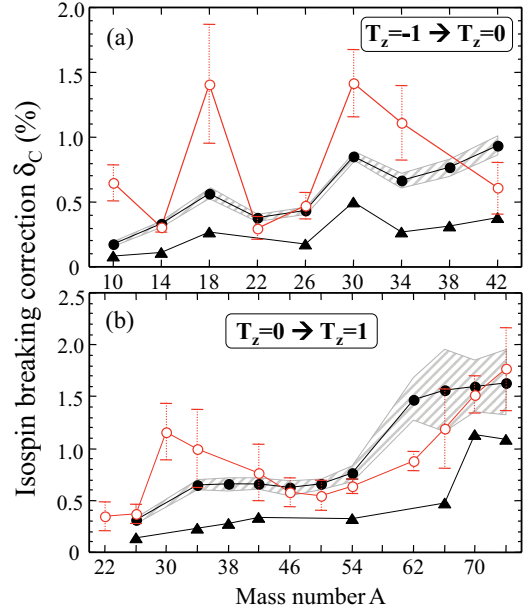


FIG. 6. (Color online) ISB corrections to superallowed $0^+ \rightarrow 0^+$ β decays calculated for (a) $T_z = -1 \rightarrow T_z = 0$ and (b) $T_z = 0 \rightarrow T_z = 1$ transitions. Our adopted values from Table II (open circles with error bars) are compared with ISB corrections from Refs. [2] (filled circles; shaded band marks errors) and [12] (filled triangles).

more sensitive to time-odd polarizations than other s.p. states around the ^{40}Ca core (see Table I in Ref. [38]). The calculated equilibrium deformations (β_2, γ) of the $T_z \pm 1$ and $T_z = 0$, $A = 38$ isobaric triplet are very similar, around $(0.090, 60^\circ)$. In the following, the $^{38}\text{K} \rightarrow ^{38}\text{Ar}$ transition is excluded from the calculation of the V_{ud} matrix element.

D. Survey of ISB corrections in $10 \leq A \leq 74$ nuclei

The results of our calculations are collected in Tables II and III and in Fig. 6. In addition, Fig. 7 shows the differences, $\delta_C^{(SV)} - \delta_C^{(HT)}$, between our results and those in Ref. [2]. In spite of clear differences between SV and HT, which can be seen for specific transitions including those for $A = 10, 34$, and 62 , both calculations reveal a similar increase in δ_C versus A , at variance with the RPA calculations in Ref. [12], which also yield systematically smaller values.

The ISB corrections used for further calculations of V_{ud} are listed in Table II. Let us recall that our preference is to use the averaged corrections and that the $^{38}\text{K} \rightarrow ^{38}\text{Ar}$ transition has been disregarded. All other ingredients needed to compute the $\mathcal{F}t$ values, including radiative corrections δ'_R and δ_{NS} , are taken from Ref. [2], and the empirical ft values are taken from Ref. [4]. For the sake of completeness, these empirical ft values are also listed in Table II.

In the error budget of the resulting $\mathcal{F}t$ values listed in Table II, apart from errors in the ft values and radiative corrections, we also included the uncertainties estimated for the calculated values of δ_C (see Sec. III C). To conform with HT, the average value $\overline{\mathcal{F}t} = 3073.6(12)\text{s}$ was calculated using the Gaussian-distribution-weighted formula. However, unlike

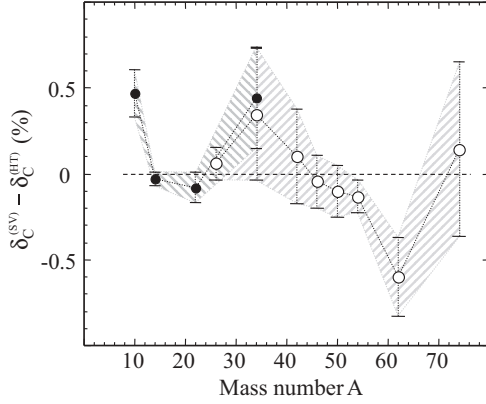


FIG. 7. Differences between the ISB corrections to the 12 accurately measured superallowed $0^+ \rightarrow 0^+$ β transitions (excluding $A = 38$) calculated in this work with SV and those of HT [2]. Open and filled circles mark the $T_z = -1 \rightarrow T_z = 0$ and $T_z = 0 \rightarrow T_z = 1$ decays, respectively. Errors, calculated as $\sqrt{(\Delta\delta_C^{(SV)})^2 + (\Delta\delta_C^{(HT)})^2}$, are shown by shaded bands.

HT, we do not apply any further corrections to \overline{Ft} . This leads to $|V_{ud}| = 0.97397(27)$, which agrees very well with both the HT result [2], $|V_{ud}^{(HT)}| = 0.97418(26)$, and the central value obtained from the neutron decay, $|V_{ud}^{(v)}| = 0.9746(19)$ [9]. A survey of the $|V_{ud}|$ values deduced using different methods is given in Fig. 8. By combining the value of $|V_{ud}|$ calculated here with those of the 2010 Particle Data Group [9], $|V_{us}| = 0.2252(9)$ and $|V_{ub}| = 0.00389(44)$, one obtains

$$|V_{ud}|^2 + |V_{us}|^2 + |V_{ub}|^2 = 0.99935(67), \quad (20)$$

which implies that the unitarity of the first row in the CKM matrix is satisfied with a precision better than 0.1%. A survey of the unitarity condition, (20), is shown in Fig. 9.

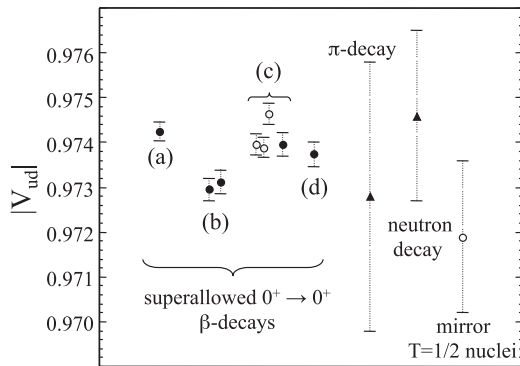


FIG. 8. The matrix element $|V_{ud}|$ deduced from the superallowed $0^+ \rightarrow 0^+$ β decay (filled circles) for different sets of the δ_C corrections calculated in (a) Ref. [2]; (b) Ref. [12] with NL3 and DD-ME2 Lagrangians; and this work, using the averaged values of δ_C with (c) SV and (d) SHZ2 functionals. Shaded circles show ISB corrections with SV calculated at fixed shape-current orientations X , Y , and Z (from left to right). Filled triangles mark values obtained from pion-decay [39] and neutron-decay [9] studies. The open circle shows the $|V_{ud}|$ deduced from β decays in $T = 1/2$ mirror nuclei [40].

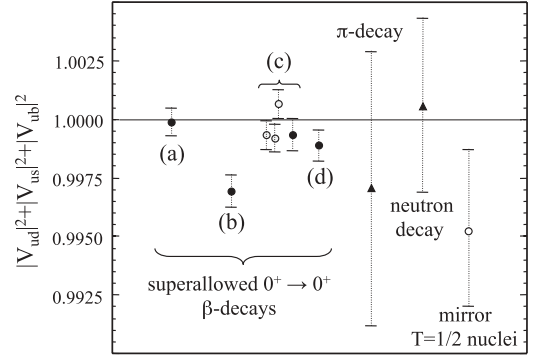


FIG. 9. Similar to Fig. 8 except for the unitarity condition, (20).

It is worth noting that by using δ_C values corresponding to the fixed current-shape orientations ($|\varphi_X$), ($|\varphi_Y$), or ($|\varphi_Z$) instead of their average, one still obtains compatible results for $|V_{ud}|$ and unitarity condition (20) (see Figs. 8 and 9). Moreover, the value of $|V_{ud}|$ obtained by using SHZ2 is only $\approx 0.024\%$ smaller than the SV result (see Table II). This is an intriguing result, which indicates that an increase in the bulk symmetry energy—which tends to restore the isospin symmetry—is partly compensated by other effects. The most likely origin of this compensation mechanism is caused by the time-odd spin-isospin MFs, which are poorly constrained by the standard fitting protocols of Skyrme EDFs [41–43]. For instance, if one compares the Landau-Migdal parameters characterizing the spin-isospin time-odd channels [41–43] of SV ($g_0 = 0.57$, $g'_0 = 0.31$, $g_1 = 0.46$, $g'_1 = 0.46$) and SHZ2 ($g_0 = 0.27$, $g'_0 = 0.30$, $g_1 = 0.47$, $g'_1 = 0.47$), one notices that these two functionals differ by a factor of 2 in the scalar-isoscalar Landau-Migdal parameter g_0 .

To illustrate the compensation mechanism related to the bulk symmetry energy and g_0 , in Fig. 10 we plot δ_C for the $^{14}\text{O} \rightarrow ^{14}\text{N} \rightarrow ^{14}\text{C}$ superallowed $0^+ \rightarrow 0^+$ transitions as functions of the bulk symmetry parameter a_{sym} for a set of SV-based Skyrme forces with a systematically varied x_0

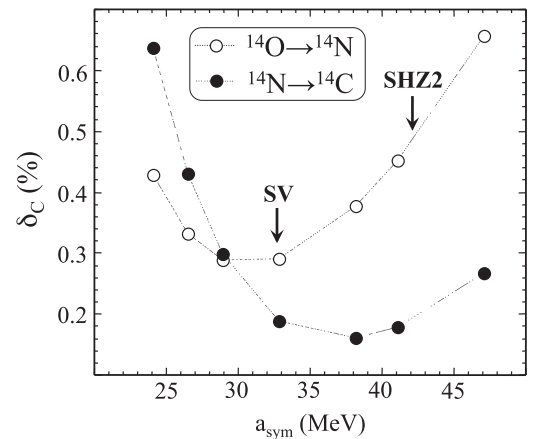


FIG. 10. ISB corrections for $^{14}\text{O} \rightarrow ^{14}\text{N}$ and $^{14}\text{N} \rightarrow ^{14}\text{C}$ superallowed $0^+ \rightarrow 0^+$ β decays calculated for a set of SV-based Skyrme forces with a systematically varied x_0 parameter, which affects the bulk asymmetry energy coefficient a_{sym} and spin-spin fields. Arrows indicate x_0 values corresponding to SV and SHZ2.

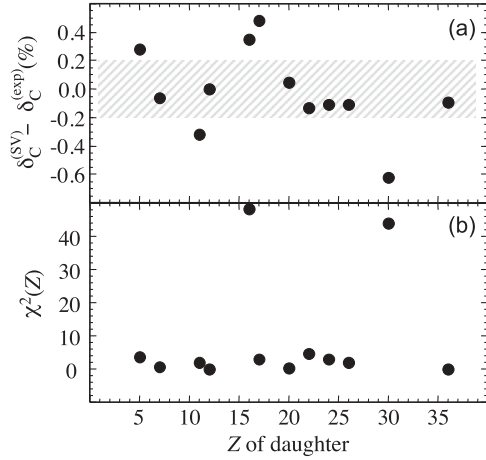


FIG. 11. Top: Differences between calculated ISB corrections and empirical values resulting from the CL test in Ref. [4]. The shaded area, of width $\pm 0.2\%$, is added in order to better illustrate the differences. Bottom: Contributions from individual transitions to the χ^2 budget. Note the particularly large contributions from the $^{34}\text{Cl} \rightarrow ^{34}\text{S}$ and $^{62}\text{Ga} \rightarrow ^{62}\text{Zn}$ transitions, which deteriorate the CL test. See text for details.

parameter. At a functional level, x_0 affects only two Skyrme coupling constants (see, e.g., Appendix A in Ref. [20]):

$$C_1^p = -\frac{1}{4}t_0 \left(\frac{1}{2} + x_0 \right) - \frac{1}{24}t_3 \left(\frac{1}{2} + x_3 \right) \rho_0^\alpha, \quad (21)$$

$$C_0^s = -\frac{1}{4}t_0 \left(\frac{1}{2} - x_0 \right) - \frac{1}{24}t_3 \left(\frac{1}{2} - x_3 \right) \rho_0^\alpha. \quad (22)$$

The coupling constant C_1^p influences the isovector part of the bulk symmetry energy [44], while C_0^s affects g_0 . The ISB correction in Fig. 10 exhibits a minimum indicating the presence of the compensation effect. A similar effect was calculated for $A = 34$ transitions. Hence, it is safe to state that our exploratory calculations are indicative of the interplay between the symmetry energy and time-odd fields.

E. Confidence-level test

In this section, we present results of the confidence-level (CL) test proposed in Ref. [4]. The CL test is based on the assumption that the CVC hypothesis is valid up to at least $\pm 0.03\%$, which implies that a set of structure-dependent corrections should produce a statistically consistent set of $\mathcal{F}t$ values. Assuming the validity of the calculated corrections δ_{NS} [6], the empirical ISB corrections can be defined as

$$\delta_C^{(\text{exp})} = 1 + \delta_{\text{NS}} - \frac{\overline{\mathcal{F}t}}{ft(1 + \delta'_R)}. \quad (23)$$

By least-squares minimization of the appropriate χ^2 , and treating the value of $\overline{\mathcal{F}t}$ as a single adjustable parameter, one can attempt to bring the set of empirical values $\delta_C^{(\text{exp})}$ as close as possible to the set of δ_C .

The empirical ISB corrections deduced in this way are listed in Table II and illustrated in Fig. 11. Table II also lists individual contributions to the χ^2 budget. The obtained χ^2 per degree of freedom ($n_d = 11$) is $\chi^2/n_d = 10.2$. This number is

twice as large as that quoted in our previous work [15], because of the large uncertainty of δ_C for the $^{34}\text{Cl} \rightarrow ^{34}\text{S}$ transition. Other than that, both previous and present calculations have difficulty in reproducing the strong increase for $A = 62$. Our χ^2/n_d is also higher than the perturbative-model values reported in Ref. [4] ($\chi^2/n_d = 1.5$), the shell model with Woods-Saxon (SM-WS) radial wave functions (0.4) [2], the shell model with radial wave functions (2.0) [3,45], the Skyrme-HF with RPA (2.1) [11], and the relativistic HF plus RPA model [12], which yields $\chi^2/n_d = 1.7$.

It is worth noting that after disregarding the two transitions that strongly violate the CVC hypothesis, $^{34}\text{Cl} \rightarrow ^{34}\text{S}$ and $^{62}\text{Ga} \rightarrow ^{62}\text{As}$, and then performing a new CL test for the remaining 10 transitions ($n_d = 9$), the normalized χ^2 drops to 1.9. Within this restricted set of data, the calculated $|V_{\text{ud}}| = 0.97420(28)$ and unitarity condition $0.99978(68)$ almost perfectly match the results in Ref. [2].

F. ISB corrections in $78 \leq A \leq 98$ nuclei

Our projected DFT approach can be used to predict isospin mixing in heavy nuclei. The calculated ISB corrections and Q values in $78 \leq A \leq 98$ nuclei are listed in Table IV. The values of δ_C are also shown in Fig. 12. Note that the predicted ISB corrections here are considerably smaller than those in $A = 70$ and $A = 74$ nuclei (see Tables II and III). For the sake of comparison, Fig. 12 also shows predictions of Ref. [46] for the $^{82}\text{Nb} \rightarrow ^{82}\text{Zr}$ transition using the VAMPIR approach with either the charge-independent Bonn A potential or the charge-dependent Bonn CD potential. Note that our prediction is only slightly below the Bonn A result and significantly lower than the Bonn CD value. For the sake of completeness, it should be mentioned that our Q_β value of 10.379 MeV for this transition agrees well with the $Q_\beta = 10.496$ MeV (Bonn A) and 10.291 MeV (Bonn CD) calculated within the VAMPIR approach.

Our calculated values of δ_C in heavy nuclei are considerably smaller than those obtained from a perturbative expression [4,10,47],

$$\delta_C = 0.002645 \frac{Z^2}{A^{2/3}} (n+1)(n+\ell+3/2) (\%), \quad (24)$$

where n and ℓ denote the number of radial nodes and angular momentum of the valence s.p. spherical wave function, respectively. Indeed, assuming the valence $1p_{1/2}$ state in $A = 78$, Eq. (24) yields $\delta_C = 1.54\%$. In heavier nuclei, where the spherical valence state is $0g_{9/2}$, Eq. (24) gives δ_C values that increase smoothly from 1.30% in $A = 82$ to 1.64% in $A = 98$.

IV. ISB CORRECTIONS TO FERMION MATRIX ELEMENTS IN MIRROR-SYMMETRIC $T = 1/2$ NUCLEI

Transitions between the isobaric analog states in mirror nuclei $|T = 1/2, I, T_z = -1/2\rangle \rightarrow |T = 1/2, I, T_z = +1/2\rangle$ offer an alternative way to extract the $\mathcal{F}t$ values [48] and V_{ud} [40,49]. Those transitions are mixed Fermi and Gamow-Teller, meaning that they are mediated by both vector and axial-vector

TABLE IV. Results of calculations for superallowed β decays in $78 \leq A \leq 98$ nuclei: isospin impurities in parent and daughter nuclei; δ_C for different shape-current orientations; averaged (recommended) δ_C ; calculated equilibrium deformations β_2 and γ ; and Q_β values calculated here and estimated from the extrapolated masses in Ref. [36].

| $T_z = 0 \rightarrow T_z = 1$ | $\alpha_C^{(P)}$ (%) | $\alpha_C^{(D)}$ (%) | $\delta_C^{(X)}$ (%) | $\delta_C^{(Y)}$ (%) | $\delta_C^{(Z)}$ (%) | $\delta_C^{(SV)}$ (%) | $\beta_2^{(SV)}$ | $\gamma^{(SV)}$ (deg) | $Q_\beta^{(th)}$ (MeV) | $Q_\beta^{(exp)}$ (MeV) |
|---|-------------------------|-------------------------|-------------------------|-------------------------|-------------------------|--------------------------|------------------|--------------------------|---------------------------|----------------------------|
| $^{78}\text{Y} \rightarrow ^{78}\text{Sr}$ | 2.765 | 0.976 | 1.20 | 1.19 | 1.20 | 1.20(12) | 0.004 | 60.0 | 10.471 | 10.650 [#] |
| $^{82}\text{Nb} \rightarrow ^{82}\text{Zr}$ | 3.099 | 1.408 | 0.70 | 0.91 | 0.70 | 0.77(13) | 0.036 | 60.0 | 10.379 | 11.220 [#] |
| $^{86}\text{Tc} \rightarrow ^{86}\text{Mo}$ | 3.337 | 1.518 | 0.89 | 0.89 | 1.08 | 0.95(13) | 0.122 | 0.0 | 10.965 | 11.350 [#] |
| $^{90}\text{Rh} \rightarrow ^{90}\text{Ru}$ | 3.525 | 1.608 | 0.99 | 0.99 | 1.09 | 1.02(11) | 0.161 | 0.0 | 11.465 | 12.090 [#] |
| $^{94}\text{Ag} \rightarrow ^{94}\text{Pd}$ | 3.674 | 1.689 | 0.86 | 0.86 | 1.17 | 0.96(18) | 0.136 | 0.0 | 11.896 | 13.050 [#] |
| $^{98}\text{In} \rightarrow ^{98}\text{Cd}$ | 3.805 | 1.771 | 0.89 | 0.89 | 1.36 | 1.05(25) | 0.057 | 0.0 | 12.343 | 13.730 [#] |

currents. Hence, the extraction of V_{ud} requires—in addition to lifetimes and Q values—measuring another observable, such as the β -neutrino correlation coefficient, β asymmetry, or the neutrino-asymmetry parameter [50,51]. Moreover, the method depends on the radiative and ISB corrections to both the Fermi and the Gamow-Teller matrix elements. In spite of these difficulties, the current precision of determination of V_{ud} using the mirror-decay approach is similar to that offered by neutron-decay experiments [9,40,49] (see also Figs. 8 and 9).

Within our projected DFT model, we performed systematic calculations of ISB corrections to the Fermi matrix elements, δ_C^V , covering the mirror transitions in all $11 \leq A \leq 49$ nuclei. Calculations were based on the Slater determinants corresponding to the lowest energy, unrestricted-symmetry HF solutions. If the unrestricted-symmetry calculations did not converge, the projection was applied to the constrained HF solutions with imposed signature symmetry. These two types of solutions differ, in particular, in relative shape-current orientation, which also varies with A , depending on the s.p. orbit occupied by an unpaired nucleon. It should be emphasized, however, that the HF solutions corresponding to the β -decay partners were always characterized by the same orientation of the odd-particle alignment with respect to the body-fixed reference frame. All calculations discussed in this

section were performed using the full basis of $N = 12$ HO shells and the SV force.

The obtained values of the ISB corrections to the Fermi transitions,

$$\delta_C^V \equiv 1 - |\langle T = \frac{1}{2}, I, T_z = \mp \frac{1}{2} | \hat{T}_\mp | T = \frac{1}{2}, I, T_z = \pm \frac{1}{2} \rangle|^2, \quad (25)$$

are listed in Table V and illustrated in Fig. 13. Because the calculations were performed in a relatively large basis, the basis-cutoff-related uncertainty in δ_C^V could be reduced to approximately 5% (cf. Sec. III C). Except for one case, theoretical spins and parities of decaying states were taken equal to those found in experiments: $I_{(th)}^\pi = I_{(exp)}^\pi$ (g.s.). Only for $A = 31$ was no $I = 1/2$ component found in the HF wave function, and thus the lowest solution corresponding to $I_{(th)}^\pi = 5/2^+$ was taken instead. It should be mentioned that, owing to the poor spectroscopic quality of SV, the projected states corresponding to $I_{(exp)}^\pi$ (g.s.) are not always the lowest ones. This situation occurs for $A = 19, 25$, and 45 , where the lowest states have $I_{(th)}^\pi = 5/2^+, 1/2^+$, and $3/2^-$, and the corresponding δ_C^V values are 0.308%, 0.419%, and 0.636%, respectively. The relatively strong dependence of the calculated ISB corrections on spin is worth noting. The calculations also indicate an appreciable impact of the signature-symmetry constraint on δ_C^V , in particular, in pf -shell nuclei with $A = 45, 47$, and 49 . A similar effect was calculated for the $0^+ \rightarrow 0^+$ transitions; see the δ_C values at fixed shape-current orientations in Tables II and III.

V. THE ISB CORRECTION TO THE FERMI DECAY BRANCH IN ^{32}Cl

The V_{ud} values extracted using diverse techniques including $0^+ \rightarrow 0^+$ nuclear decays, nuclear mirror decays, neutron decay, and pion decay are subject to both experimental and theoretical uncertainties. The latter pertain to calculations of radiative processes and—for nuclear methods—to the nuclear ISB effect. The uncertainties in radiative and ISB corrections affect the overall precision of V_{ud} at the level of a few parts per 10^4 each [1,51]. It should be stressed, however, that the ISB contribution to the error bar of V_{ud} was calculated only for a single theoretical model (SM-WS). Other microscopic models, including the shell model with HF radial wave functions [3],

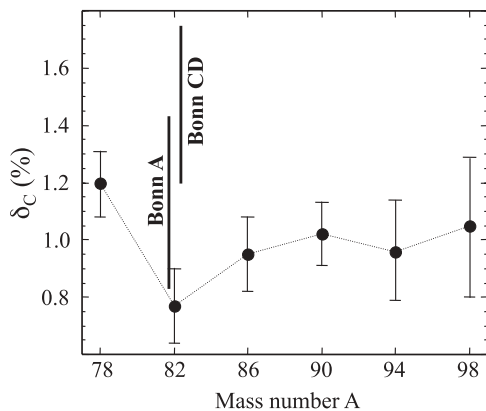


FIG. 12. ISB corrections to superallowed $0^+ \rightarrow 0^+$ transitions in heavy nuclei calculated in the present work (filled circles). Vertical bars mark ISB corrections to the $^{82}\text{Nb} \rightarrow ^{82}\text{Zr}$ transition calculated in Ref. [46] using the VAMPIR formalism with the charge-independent Bonn A and charge-dependent Bonn CD interactions.

TABLE V. Results of calculations for $|T = 1/2, I, T_z = -1/2\rangle \rightarrow |T = 1/2, I, T_z = +1/2\rangle$ β decays between mirror nuclei: theoretical spin and parity assignments; isospin-mixing coefficients in parent and daughter nuclei; ISB corrections calculated in this work (asterisks denote results obtained within unrestricted-symmetry calculations); ISB corrections from Ref. [48]; quadrupole equilibrium deformation parameters in parent nuclei; and theoretical and experimental Q_β values.

| | I^π | $\alpha_C^{(P)}$ (%) | $\alpha_C^{(D)}$ (%) | $\delta_C^{V(SV)}$ (%) | $\delta_C^{V(S)}$ (%) | $\beta_2^{(SV)}$ | $\gamma^{(SV)}$ (deg) | $Q_\beta^{(th)}$ (MeV) | $Q_\beta^{(exp)}$ (MeV) |
|---|---------|-------------------------|-------------------------|---------------------------|--------------------------|------------------|--------------------------|---------------------------|----------------------------|
| $^{11}\text{C} \rightarrow ^{11}\text{B}$ | $1/2^-$ | 0.001 | 0.003 | 0.077 | 0.928 | 0.320 | 43.8 | 1.656 | 1.983 |
| $^{13}\text{N} \rightarrow ^{13}\text{C}$ | $1/2^-$ | 0.008 | 0.001 | 0.139 | 0.271 | 0.210 | 59.1 | 1.888 | 2.221 |
| $^{15}\text{O} \rightarrow ^{15}\text{N}$ | $1/2^-$ | 0.012 | 0.002 | 0.127 | 0.181 | 0.003 | 0.0 | 2.446 | 2.754 |
| $^{17}\text{F} \rightarrow ^{17}\text{O}$ | $1/2^+$ | 0.020 | 0.031 | 0.167 | 0.585 | 0.014 | 0.0 | 2.496 | 2.761 |
| | | 0.019 | 0.029 | 0.178* | 0.585 | 0.064 | 60.0 | 2.499 | |
| $^{19}\text{Ne} \rightarrow ^{19}\text{F}$ | $1/2^+$ | 0.036 | 0.034 | 0.365 | 0.415 | 0.321 | 0.0 | 2.928 | 3.239 |
| $^{21}\text{Na} \rightarrow ^{21}\text{Ne}$ | $1/2^+$ | 0.047 | 0.052 | 0.307 | 0.348 | 0.434 | 0.0 | 3.229 | 3.548 |
| $^{23}\text{Mg} \rightarrow ^{23}\text{Na}$ | $1/2^+$ | 0.064 | 0.070 | 0.340 | 0.293 | 0.434 | 0.0 | 3.587 | 4.057 |
| $^{25}\text{Al} \rightarrow ^{25}\text{Mg}$ | $1/2^+$ | 0.073 | 0.058 | 0.503 | 0.461 | 0.444 | 1.6 | 3.683 | 4.277 |
| $^{27}\text{Si} \rightarrow ^{27}\text{Al}$ | $1/2^+$ | 0.074 | 0.073 | 0.472 | 0.312 | 0.343 | 47.7 | 4.250 | 4.813 |
| $^{29}\text{P} \rightarrow ^{29}\text{Si}$ | $1/2^+$ | 0.123 | 0.113 | 0.694 | 0.976 | 0.332 | 54.4 | 4.399 | 4.943 |
| $^{31}\text{S} \rightarrow ^{31}\text{P}$ | $1/2^+$ | 0.163 | 0.164 | 0.504 | 0.715 | 0.315 | 0.0 | 4.855 | 5.396 |
| $^{33}\text{Cl} \rightarrow ^{33}\text{S}$ | $1/2^+$ | 0.177 | 0.160 | 0.644 | 0.865 | 0.258 | 33.5 | 5.002 | 5.583 |
| $^{35}\text{Ar} \rightarrow ^{35}\text{Cl}$ | $1/2^+$ | 0.186 | 0.182 | 0.576 | 0.493 | 0.209 | 50.4 | 5.482 | 5.966 |
| $^{37}\text{K} \rightarrow ^{37}\text{Ar}$ | $1/2^+$ | 0.291 | 0.267 | 1.425 | 0.734 | 0.143 | 60.0 | 5.589 | 6.149 |
| $^{39}\text{Ca} \rightarrow ^{39}\text{K}$ | $1/2^+$ | 0.318 | 0.289 | 0.392* | 0.855 | 0.034 | 60.0 | 6.084 | 6.531 |
| $^{41}\text{Sc} \rightarrow ^{41}\text{Ca}$ | $1/2^-$ | 0.341 | 0.345 | 0.426* | 0.821 | 0.032 | 60.0 | 5.968 | 6.496 |
| $^{43}\text{Ti} \rightarrow ^{43}\text{Sc}$ | $1/2^-$ | 0.376 | 0.380 | 0.463* | 0.500 | 0.090 | 60.0 | 6.225 | 6.868 |
| $^{45}\text{V} \rightarrow ^{45}\text{Ti}$ | $1/2^-$ | 0.437 | 0.424 | 0.534 | 0.865 | 0.233 | 0.0 | 6.563 | 7.134 |
| | | 0.438 | 0.427 | 0.661* | 0.865 | 0.233 | 0.0 | 6.559 | |
| $^{47}\text{Cr} \rightarrow ^{47}\text{V}$ | $1/2^-$ | 0.480 | 0.457 | 0.518 | — | 0.276 | 0.0 | 6.827 | 7.452 |
| | | 0.483 | 0.463 | 0.710* | — | 0.275 | 0.0 | 6.826 | |
| $^{49}\text{Mn} \rightarrow ^{49}\text{Cr}$ | $1/2^-$ | 0.515 | 0.497 | 0.522 | — | 0.284 | 0.9 | 7.054 | 7.715 |
| | | 0.518 | 0.499 | 0.681* | — | 0.284 | 0.0 | 7.053 | |

RH-RPA [12], and projected DFT [15], yield δ_C corrections that may differ substantially from those obtained in SM-WS calculations.

Inclusion of the model dependence in the calculated uncertainties is expected to increase the uncertainty of V_{ud} . According to Ref. [52] the increase can reach even an order of magnitude. In our opinion, a reasonable assessment of

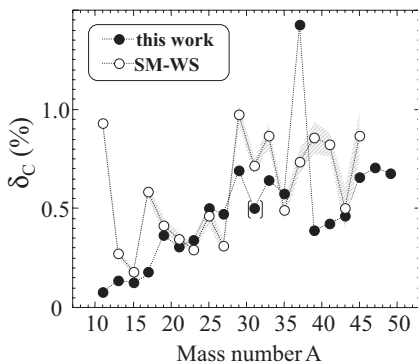


FIG. 13. Filled circles: Calculated values of ISB corrections to Fermi transitions in $T = 1/2$ mirror nuclei. Open circles with errors: Results calculated by Severijns *et al.* [48].

systematic errors (owing to the model dependence) cannot be done at present, as it requires the assumption either that all the nuclear structure models considered are equally reliable or that their performance can be graded in an objective way.

A good way to verify the reliability of various models is to compare their predictions with empirically determined δ_C . Recently, the anomalously large value of $\delta_C \approx 5.3(9)\%$ has been determined from a precision measurement of the γ yields following the β decay of the $I = 1^+$, $T = 1$ state in ^{32}Cl to its isobaric analog state (Fermi branch) in ^{32}S [53]. This value offers a stringent test of nuclear-structure models, because it is significantly larger than any value of δ_C in $A = 4n + 2$ nuclei. The physical reason for this enhancement can be traced back to a mixing of two close-lying $I = 1^+$ states seen in ^{32}S at the excitation energies of 7002 and 7190 keV, respectively [54]. The lower one is the isobaric analog state having predominantly a $T = 1$ component, while the higher one is primarily of $T = 0$ character.

The experimental value $\delta_C \approx 5.3(9)\%$ is consistent with the SM-WS calculations: $\delta_C \approx 4.6(5)\%$. In our projected DFT approach, we also see fingerprints of the strong enhancement of the δ_C value in ^{32}Cl compared to other $A = 4n + 2$ nuclei. Unfortunately, a static DFT approach based on projecting from a single reference state is not sufficient to give a reliable

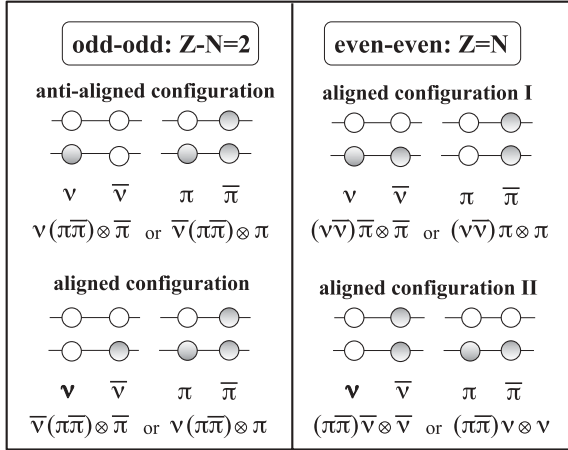


FIG. 14. Schematic of several possible mean-field configurations in odd-odd $Z - N = 2$ (left) and even-even $N = Z$ (right) nuclei. The pairs of proton (neutron) s.p. levels, labeled π and $\bar{\pi}$ (ν and $\bar{\nu}$), are assumed to be degenerated owing to the intrinsic signature symmetry. The orbits ν and π carry the signature quantum number $r = -i$ ($\alpha = 1/2$), while $\bar{\nu}$ and $\bar{\pi}$ have $r = i$ ($\alpha = -1/2$).

prediction. This is because, as sketched in Fig. 14, there exist ambiguities in selecting the HF reference state. In the extreme isoscalar s.p. scenario, by distributing four valence protons and neutrons over the Nilsson s.p. levels in an odd-odd nucleus, one can form two distinctively different s.p. configurations (see Fig. 14).

The total signature of valence particles determines the total signature of the odd-odd nucleus and, in turn, an approximate angular-momentum distribution in its wave function [55]; the total additive signature $\alpha_T(\text{mod}2) = 0(1)$ then corresponds to even (odd) spins in the wave function [56]. It is immediately seen that the antialigned configuration shown in Fig. 14 has $\alpha_T = 0$; hence, in the first approximation, it can be disregarded. In this sense, the reference wave function in ^{32}Cl (or, in general, in any $N - Z = \pm 2$ odd-odd nucleus) corresponds to the uniquely defined aligned state. As shown in Fig. 14, this does not hold for ^{32}S (or, in general, for any $N = Z$ even-even nucleus), where one must consider two possible Slater determinants having $\alpha_T = 1$, obtained by a suitable proton or neutron particle-hole excitation.

The above discussion indicates that, contrary to transitions involving the odd-odd $N = Z$ nuclei studied in Sec. III, those involving even-even $N = Z$ nuclei cannot be directly treated within the present realization of the model. To this end, the model requires enhancements including configuration mixing (multireference DFT). Nevertheless, we have carried out an exploratory study by independently calculating two ISB corrections for the two configurations discussed above. These calculations proceeded in the following way.

- (1) We select the appropriate reference configurations, which, in the present case, are $\nu[4, 5, 3, 3]\pi[5, 6, 3, 3]$ in ^{32}Cl and φ_I : $\nu[5, 5, 3, 3]\pi[4, 6, 3, 3]$ and φ_{II} : $\nu[4, 6, 3, 3]\pi[5, 5, 3, 3]$ in ^{32}S . The labels denote the numbers of neutrons and protons occupying the lowest Nilsson levels in each parity-signature block, $(\pi, r) =$

- (+), (+i), (+, -i), (-, +i), and (-, -i), counting from the bottom of the HF potential well, as defined in Ref. [57].
- (2) We determine the lowest $|I^\pi = 1^+, T \approx 1, T_z = -1\rangle$ and $|\varphi_i; I^\pi = 1^+, T \approx 1, T_z = 0\rangle$ ($i = I, II$) states by projecting onto subspaces of good angular momentum and isospin and performing K mixing and Coulomb re-diagonalization as described in Sec. II.
- (3) Finally, we calculate matrix elements of the Fermi operator \hat{T}_\pm and extract δ_C .

The resulting ISB corrections are $\delta_C^{(\varphi_I)} = 2.40(24)\%$ and $\delta_C^{(\varphi_{II})} = 4.22(42)\%$ for the φ_I and φ_{II} configurations, respectively. As before, we assumed a 10% error owing to the basis size ($N = 10$ spherical HO shells). Projections from the same configurations cranked in space to $\langle \hat{J}_y \rangle = 1\hbar$ (see discussion in Ref. [27]) leave ISB corrections almost unaffected: $\delta_C^{(\varphi_I)} = 2.41(24)\%$ and $\delta_C^{(\varphi_{II})} = 4.30(43)\%$. A simple average value would read $\delta_C = 3.4(10)\%$, which is indeed strongly enhanced compared to the $A = 4n + 2$ cases. The obtained central value is smaller than both the empirical value and the SM-WS result. It is worth noting, however, that within the stated errors our mean value, 3.4(10)%, agrees with the SM-WS value, 4.6(05)%. Whether or not the configuration-mixing calculations would provide a significant enhancement is an entirely open question.

VI. SUMMARY AND PERSPECTIVES

Within the recently developed unpaired projected DFT approach, we carried out systematic calculations of isospin mixing effects and ISB corrections to the superallowed $0^+ \rightarrow 0^+$ Fermi decays in $10 \leq A \leq 74$ nuclei and β transitions between the isobaric analog states in mirror $T = 1/2$ nuclei with $11 \leq A \leq 49$. Our predictions are compared with empirical values and with predictions of other theoretical approaches. Using ISB corrections computed in our model, we show that the unitarity of the CKM matrix is satisfied with a precision of better than 0.1%. We also provide ISB corrections for heavier nuclei with $78 \leq A \leq 98$ nuclei that can guide future experimental and theoretical studies.

We carefully analyze various model assumptions impacting theoretical uncertainties of our calculations: basis truncation, definition of the intrinsic state, and configuration selection. To assess the robustness of our results with respect to the choice of interaction, we compare SV results with predictions of the new force SHZ2, which has been specifically developed for this purpose. The comparison of SV and SHZ2 results suggests that ISB corrections are sensitive to the interplay between the bulk symmetry energy and time-odd MFs.

While the overall agreement with the empirical values offered by the projected DFT approach is very encouraging, and the results are fairly robust, there is a lot of room for systematic improvement. The main disadvantages of our model in its present formulation include (i) the lack of pairing correlations; (ii) the lack of p-h interaction (or functional) of good spectroscopic quality; (iii) the use of a single HF reference state that cannot accommodate configuration mixing effects; and (iv) ambiguities in establishing the HF

reference state in odd and odd-odd nuclei caused by different possible orientations of time-odd currents with respect to the total density distribution. Work on various enhancements of our model, including the inclusion of $T = 0$ and $T = 1$ pairing within the projected HF-Bogoliubov theory, better treatment of configuration mixing using the multireference DFT, and development of the spectroscopic-quality EDF used in projected calculations, is in progress.

ACKNOWLEDGMENTS

This work was supported in part by the Academy of Finland and University of Jyväskylä within the FIDIPRO program and by the Office of Nuclear Physics, US Department of Energy, under Contracts No. DE-FG02-96ER40963 (University of Tennessee) and No. DE-SC0008499 (NUCLEI SciDAC-3 Collaboration). We acknowledge the CSC-IT Center for Science Ltd., Finland, for the allocation of computational resources.

-
- [1] J. C. Hardy and I. S. Towner, *Phys. Rev. Lett.* **94**, 092502 (2005); *Phys. Rev. C* **71**, 055501 (2005).
- [2] I. S. Towner and J. C. Hardy, *Phys. Rev. C* **77**, 025501 (2008).
- [3] J. C. Hardy and I. S. Towner, *Phys. Rev. C* **79**, 055502 (2009).
- [4] I. S. Towner and J. C. Hardy, *Phys. Rev. C* **82**, 065501 (2010).
- [5] W. J. Marciano and A. Sirlin, *Phys. Rev. Lett.* **96**, 032002 (2006).
- [6] I. S. Towner, *Phys. Lett. B* **333**, 13 (1994).
- [7] N. Cabibbo, *Phys. Rev. Lett.* **10**, 531 (1963).
- [8] M. Kobayashi and T. Maskawa, *Prog. Theor. Phys.* **49**, 652 (1973).
- [9] K. Nakamura and Particle Data Group, *J. Phys. G* **37**, 075021 (2010).
- [10] J. Damgaard, *Nucl. Phys. A* **130**, 233 (1969).
- [11] H. Sagawa, N. V. Giai, and T. Suzuki, *Phys. Rev. C* **53**, 2163 (1996).
- [12] H. Liang, N. Van Giai, and J. Meng, *Phys. Rev. C* **79**, 064316 (2009).
- [13] N. Auerbach, *Phys. Rev. C* **79**, 035502 (2009).
- [14] W. Satuła, J. Dobaczewski, W. Nazarewicz, and M. Rafalski, *Int. J. Mod. Phys. E* **20**, 244 (2011).
- [15] W. Satuła, J. Dobaczewski, W. Nazarewicz, and M. Rafalski, *Phys. Rev. Lett.* **106**, 132502 (2011).
- [16] W. Satuła, J. Dobaczewski, W. Nazarewicz, and M. Rafalski, *Acta Phys. Pol. B* **42**, 415 (2011).
- [17] M. Rafalski and W. Satuła, *Phys. Scripta T* **150**, 014032 (2012).
- [18] C. Yannouleas and U. Landman, *Rep. Prog. Phys.* **70**, 2067 (2007).
- [19] S. Frauendorf, *Rev. Mod. Phys.* **73**, 463 (2001).
- [20] M. Bender, P.-H. Heenen, and P.-G. Reinhard, *Rev. Mod. Phys.* **75** (2003).
- [21] W. Satuła and R. Wyss, *Rep. Prog. Phys.* **68**, 131 (2005).
- [22] P. Ring and P. Schuck, *The Nuclear Many-Body Problem* (Springer, Berlin, 1980).
- [23] W. Satuła, J. Dobaczewski, W. Nazarewicz, and M. Rafalski, *Phys. Rev. Lett.* **103**, 012502 (2009).
- [24] W. Satuła, J. Dobaczewski, W. Nazarewicz, and M. Rafalski, *Phys. Rev. C* **81**, 054310 (2010).
- [25] D. Varshalovich, A. Moskalev, and V. Khersonskii, *Quantum Theory of Angular Momentum* (World Scientific, Singapore, 1988).
- [26] J. Dobaczewski, W. Satuła, B. G. Carlsson, J. Engel, P. Olbratowski, P. Powłowski, M. Sadziak, J. Sarich, N. Schunck, A. Staszczak, M. Stoitsov, M. Zalewski, and H. Zduńczuk, *Comput. Phys. Commun.* **180**, 2361 (2009).
- [27] H. Zduńczuk, W. Satuła, J. Dobaczewski, and M. Kosmulski, *Phys. Rev. C* **76**, 044304 (2007).
- [28] W. E. Ormand and B. A. Brown, *Phys. Rev. C* **52**, 2455 (1995).
- [29] G. A. Miller and A. Schwenk, *Phys. Rev. C* **78**, 035501 (2008); **80**, 064319 (2009).
- [30] J. A. Sheikh and P. Ring, *Nucl. Phys. A* **665**, 7 (2000).
- [31] M. Anguiano, J. L. Egido, and L. M. Robledo, *Nucl. Phys. A* **696**, 467 (2001).
- [32] D. Lacroix, T. Duguet, and M. Bender, *Phys. Rev. C* **79**, 044318 (2009).
- [33] A. Corsi *et al.*, *Phys. Rev. C* **84**, 041304 (2011).
- [34] J. Dobaczewski, M. V. Stoitsov, W. Nazarewicz, and P.-G. Reinhard, *Phys. Rev. C* **76**, 054315 (2007).
- [35] M. Beiner, H. Flocard, N. V. Giai, and P. Quentin, *Nucl. Phys. A* **238**, 29 (1975).
- [36] G. Audi, A. H. Wapstra, and C. Thibault, *Nucl. Phys. A* **729**, 337 (2003).
- [37] N. Schunck, J. Dobaczewski, J. McDonnell, W. Satuła, J. Sheikh, A. Staszczak, M. Stoitsov, and P. Toivanen, *Comput. Phys. Commun.* **183**, 166 (2012).
- [38] M. Zalewski, J. Dobaczewski, W. Satuła, and T. R. Werner, *Phys. Rev. C* **77**, 024316 (2008).
- [39] D. Počanić *et al.*, *Phys. Rev. Lett.* **93**, 181803 (2004).
- [40] O. Naviliat-Cuncic and N. Severijns, *Phys. Rev. Lett.* **102**, 142302 (2009).
- [41] F. Osterfeld, *Rev. Mod. Phys.* **64**, 491 (1992).
- [42] M. Bender, J. Dobaczewski, J. Engel, and W. Nazarewicz, *Phys. Rev. C* **65**, 054322 (2002).
- [43] H. Zduńczuk, W. Satuła, and R. A. Wyss, *Phys. Rev. C* **71**, 024305 (2005).
- [44] W. Satuła, R. A. Wyss, and M. Rafalski, *Phys. Rev. C* **74**, 011301 (2006).
- [45] W. E. Ormand, *Phys. Rev. C* **53**, 214 (1996).
- [46] A. Petrovici, K. W. Schmid, O. Radu, and A. Faessler, *Phys. Rev. C* **78**, 064311 (2008).
- [47] I. Towner, J. Hardy, and M. Harvey, *Nucl. Phys. A* **284**, 269 (1977).
- [48] N. Severijns, M. Tandecki, T. Phalet, and I. S. Towner, *Phys. Rev. C* **78**, 055501 (2008).
- [49] O. Naviliat-Cuncic and N. Severijns, *Eur. Phys. J. A* **42**, 327 (2009).
- [50] N. Severijns, M. Beck, and O. Naviliat-Cuncic, *Rev. Mod. Phys.* **78**, 991 (2006).
- [51] I. S. Towner and J. C. Hardy, *Rep. Prog. Phys.* **73**, 046301 (2010).
- [52] H. Liang, N. V. Giai, and J. Meng, *J. Phys. Conf. Ser.* **321**, 012055 (2011).
- [53] D. Melconian *et al.*, *Phys. Rev. Lett.* **107**, 182301 (2011).
- [54] C. Ouellet and B. Singh, *Nuclear Data Sheets* **12**, 2199 (2011).
- [55] R. Bengtsson and H.-B. Håkansson, *Z. Phys. A* **288**, 193 (1978).
- [56] A. Bohr and B. R. Mottelson, *Nuclear Structure, Vol. II* (W. A. Benjamin, Reading, MA, 1975).
- [57] J. Dobaczewski and J. Dudek, *Comput. Phys. Commun.* **131**, 164 (2000).